Electrocatalysis
DOI 10.1007/s12678-014-0184-3

Agglomeration and Cleaning of Carbon Supported Palladium Nanoparticles in Electrochemical Environment

Cauê A. Martins · Pablo S. Fernández · Horacio E. Troiani · Maria E. Martins · Ana Arenillas · Giuseppe A. Camara

Abstract Here we investigate the electrochemical behavior of Pd/C synthesized by reduction with ethylene glycol in the presence of polyvinylpyrrolidone (EG-PVP). EG-PVP produces nanoparticles (NPs) with a narrow size distribution, but some of them remain covered by impurities after the synthesis. After successive voltammetric cycles, NPs become cleaner, but some agglomeration and structural modification occur; these effects affect the electrochemical behavior of Pd/C in different ways, so we used CO as a probe to better understand the processes taking place. CO stripping shows that the general features of the multiple oxidation peaks change with the number of cycles. Possibly, CO and OH from different NPs react when the particles agglomerate, contributing to CO stripping changes. Finally, different active areas are found when the charges involved in CO oxidation and PdO reduction are compared. Such differences are rationalized in terms of a balance between the increase of sites which promote the oxidation of CO and the loss of area provoked by the growing of the particles.

Keywords Palladium nanoparticles · PVP · Cleaning process · Agglomeration of nanoparticles · Active surface area · CO probe

Electronic supplementary material The online version of this article (doi:10.1007/s12678-014-0184-3) contains supplementary material, which is available to authorized users.

C. A. Martins (✉) · G. A. Camara (✉)
Institute of Chemistry, Universidade Federal de Mato Grosso do Sul, P.O. Box 549, 79070-900 Campo Grande, Mato Grosso do Sul, Brazil
e-mail: caualvesmartins@gmail.com
e-mail: giuseppe.silva@ufms.br

P. S. Fernández · M. E. Martins
Instituto de Investigaciones Fisicoquímicas Teóricas y Aplicadas (INIFTA), Facultad de Ciencias Exactas, CONICET, CCT La Plata, UNLP, 1900 La Plata, Argentina

H. E. Troiani
División Metales, Centro Atómico Bariloche, Av. Ezequiel Bustillo 9500, San Carlos de Bariloche 8400, Río Negro, Argentina

A. Arenillas
Department of Energy and Environment, Instituto Nacional del Carbón, CSIC, Apartado 73, 33080 Oviedo, Spain

Introduction

Fuel cells fed with H_2 are an outstanding energetic alternative to the production of energy from fossil fuels. In this sense, Pt-based materials have been extensively studied as possible electrocatalysts in low-temperature fuel cells, especially for the electrooxidation of hydrogen. However, obtaining pure H_2 from electrolysis of water is an expensive process, and the production of H_2 from hydrocarbons catalytic reform generates impurities, particularly CO, which can strongly bind to the surface of the catalyst and compromise the performance of the fuel cell [1]. Due to these issues (and others, like the costs of Pt-based catalysts), researchers have been dedicated to develop Pd-based catalysts tolerant to the presence of CO [2, 3]. In this sense, it is well-known that experimental conditions adopted during the synthesis of a catalyst strongly influence its activity [2, 3].

The use of polyvinylpyrrolidone (PVP) combined with the chemical reduction method induced by polyols was firstly developed by Chen and Xing for the synthesis of platinum nanoparticles (NPs) and since then it has been widely used [4]. This simple method of synthesis combines reproducibility, quickness, and generates well dispersed NPs over different kinds of carbon substrates with a relative narrow size distribution [5–7]. However, aside from the difficulty of understanding the behavior of NPs, this method adds other complex variable, the PVP. In this regard, recent papers reported the

Published online: 16 January 2014

interaction of PVP and other surfactants with the surface of NPs [8–10] and its influence on the electrocatalytic activity of these materials [11, 12]. Tremiliosi-Filho et al. investigated the electrochemical behavior of PVP on polycrystalline Pt and Pt single crystals [11]. They showed that PVP hampered the characteristic hydrogen UPD and anion adsorption on all investigated surfaces [11]. Stamenkovic et al. showed that NPs with surfactants cannot be directly used as catalysts [8]. They studied the effect of surfactant removal on the electrocatalytic performance of Pt NPs prepared by organic synthesis [8]. Among the methods studied, low-temperature thermal annealing in air was found to be the most effective for cleaning of the surface without inducing changes in the particle size or in the morphology of the NPs [8]. Gong et al. used stripping of CO as a possible method to remove PVP from the surface of nanoparticles [10].

In this context, a complicating factor is that ethylene glycol (EG), the alcohol commonly used for the reduction step, produces glycolate, which in turn plays the role of a surfactant covering the metal surface [13]. Hence, one important attempt to minimize the side effects caused by the presence of these inevitable synthesis impurities is the development of electrochemical protocols to clean the surface of NPs [14, 15] previous to its use as catalysts in fuel cells (since potential cycling is not applicable to fuel cells).

Nevertheless, the potential cycling of the NPs might be accompanied by other processes which can cause important changes in their electrochemical behavior [15], namely (a) loss of mass due to the oxidation of the NPs during a cyclic voltammogram, (b) Ostwald ripening: the oxidation of NPs leads to the production of ions which redeposit rather over larger NPs [16], (c) a possible structural reorganization of the surface of NPs due to the exit of the surfactant, and (d) NPs can be detached from the substrate during application of potential cycling [17].

In this context, CO appears as a useful probe molecule in characterization studies once its electrooxidation is very sensitive to the characteristics of the surface. For instance, Savinova et al. ascribe the multiplicity of oxidation peaks observed during the stripping of a CO monolayer on Pt to the existence of NPs with several sizes and shapes [18, 19]. Furthermore, other works showed that the CO electrooxidation is anticipated (i.e., the corresponding oxidation peaks are observed at lower potentials) as NPs agglomerate [20–22]. In addition, studies with Pt NPs showed that for those of ~1–2 nm of diameter, CO is mostly adsorbed in an on-top configuration, but with the increase of the NP size, the fraction of bridge-bonded CO grows [23, 24].

These extensive series of data make clear that the intrinsic catalytic activity of a surface can only be accessed if the superficial and morphological parameters are taken into account and followed during the acquisition of electrochemical data. In this context, herein we investigate the effect of potential cycling in alkaline media on Pd/C nanoparticles synthetized by polyol method using PVP and how eventual changes affect the electrooxidation of CO. In order to achieve that, we submit the catalyst to successive voltammetric cycles to obtain clean NPs while we followed its electrochemical behavior. We also monitored the electrochemically active surface area (EASA) by two methods commonly used in electrocatalysis and discussed the changes observed in terms of surface cleaning and agglomeration of the nanoparticles.

Experimental

Solutions were prepared using ethylene glycol (Vetec), polyvinylpyrrolidone (40,000 g mol^{-1}, Sigma Aldrich), $PdCl_2$ (Sigma Aldrich), and 2-propanol (Sigma Aldrich). For the experiments, we used NaOH (Sigma Aldrich) 0.1 mol L^{-1} prepared with Milli-Q® water (18.2 MΩ cm). The solutions were purged with N_2 (99.99 % of purity) before and during the electrochemical experiments.

Pd/C Nanoparticles

The synthesis of NPs dispersed on carbon Vulcan XC72® was made as described elsewhere [4], with slight differences. An aqueous dispersion containing 2 mmol L^{-1} of $PdCl_2$, carbon Vulcan® XC-72R, and PVP was mixed to a solution containing ethylene glycol/water 3:1 (*v*/*v*) and heated under 150 °C for 2 h. The PVP/metal molar ratio was set to 0.3, and the amount of palladium was calculated to obtain a metal load of 20 % (*w*/*w*) in the catalyst. Afterward, this dispersion was washed with water and centrifuged at 4,500 rpm for 1 h. The process was repeated five times, and the remaining dispersion was finally dried under 60 °C for 24 h. For preparing the working electrodes, Pd/C was deposited on a polycrystalline gold disk (polished to a mirror finish) as follows: An ink was prepared by mixing 1 mg of the Pd/C powder dispersed in 2 mL of 2-propanol and 50 μL Nafion® 5 % (*v*/*v*), followed by sonication for 30 min. Meanwhile the gold disk (0.79 cm^2 of geometric area) was kept at 50±2 °C. Then, an aliquot of 200 μL from the dispersion and 50 μL of diluted Nafion® solution (1 mL of Nafion® 5 %:20 mL of 2-propanol) was dripped over the disk. Before each experiment, the electrode was rinsed with water jets in order to pull out those particles not well adhered to the surface.

Electrochemical Experiments

The experiments were performed in a three-electrode cell in NaOH 0.1 mol L^{-1}. A Pt plate was used as counter electrode, and all the potentials were measured against a Hg/HgO electrode but are presented with respect to the reversible hydrogen electrode (RHE) scale.

The electrooxidation of CO was carried out at 0.02 V s^{-1} before potential cycling and after 10, 20, 50, 100, 200, and 500 consecutive cycles between 0.1 and 1.5 V vs. RHE. The cyclic voltammograms in the absence of CO were obtained at 0.1 V s^{-1} in the same potential range.

Transmission Electron Microscopy

Transmission electron microscopy (TEM) and high-resolution transmission electron microscopy (HRTEM) analyses were performed in fresh and after cycled Pd/C catalysts. These experiments were carried out in a CM 200 Philips transmission electron microscope, which operates with a LaB_6 emission gun. The microscope is equipped with an ultratwin objective lens, and it was operated at 200 keV.

X-ray Diffraction Patterns

The diffractograms of the fresh powder were recorded in a Bruker D8 powder diffractometer equipped with a monochromatic Cu Ka X-ray source and an internal standard of silicon powder. The diffractometer is also equipped with a Göbel mirror in the incident beam and a parallel-slits analyzer in the diffracted beam. Diffraction data were collected by step scanning with a step size of 0.02° in the range of 5–90°, with an interval of 2 s between steps.

Results and Discussion

Physical Characterization

X-ray diffraction pattern of Pd/C is shown in Fig. 1. The X-ray spectrum shows a peak corresponding to the Vulcan XC72® and Pd nanoparticles. The (002) reflection peak confirms the presence of graphitic planes in the structure of the carbon support. All the other peaks refer to palladium NPs. By applying the Bragg equation to the (220) reflection peak, we estimated the Pd lattice parameter as 0.389 nm. This value is in reasonable agreement with that reported by Jaeger et al. [25]. The broadening of the peaks is mainly due to the small particles size. We estimated the average size of the crystallites (6.2 nm) by applying the Scherrer equation to all the reflection peaks. The result is consistent with the value of the particle size for the fresh catalyst obtained from TEM images for the same sample.

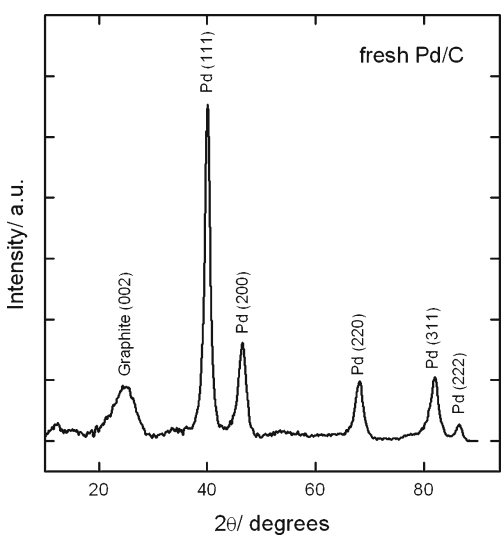

Fig. 1 X-ray diffraction spectrum for carbon supported palladium NPs

Electrochemical Cleaning of Pd/C Nanoparticles

The fresh Pd/C nanoparticle catalyst (Pd/C-0) was characterized by TEM and HRTEM (Fig. 2a, b, respectively). The images show well-dispersed NPs, although there are points of agglomeration (Fig. 2a). HRTEM results (Fig. 2b) show that NPs do not present a uniform shape, although most of them are nearly spherical.

For Pd/C-0, a mean diameter of 5.3±1.9 nm was determined by measuring 200 NPs using the software Axio Vision SE64 Rel.4.8. The corresponding histograms and their description (including major details of Fig. 2) will be resumed later in the text.

As described in the experimental section, Pd/C NPs were submitted to successive voltammetric cycles. Representative voltammograms of the Pd/C profile in NaOH 0.1 mol L^{-1} are shown in Fig. 3. The peaks associated with the electrodesorption of H atoms on palladium surface are present as two small shoulders at ~0.4 and 0.53 V (Fig. 3, black line). During the reverse sweep, the palladium oxide begins to be reduced at ~0.84 V, peaking at 0.52 V. In a general way, the profile is similar to the one described by Bolzán for bulk palladium electrodes, including the slightly negative current at low potentials [26]. As the catalyst is cycled, the peak related to desorption of H displaces toward more positive potentials and currents at ~1.3 V, commonly associated to the formation of PdO, decrease. At the initial stage, part of the oxidation charge observed at high potentials is probably caused by the oxidation of synthesis residues [13]. These currents decrease in function of the potential cycling, due to the cleaning process [15]. On the other hand, PdO reduction peak centered at ~0.5 V increases up to a maximum and decreases posteriorly. The peaks of formation and reduction of PdO display different behavior; the obvious reason is that the impurities removed from surface are not reduced during the reverse scan. However, the impurity removal increases the amount of active sites available to form surface oxides, which explain the increase of the PdO reduction peak. Further details about the PdO reduction peak and the potential shift of the H region will be seen throughout the text.

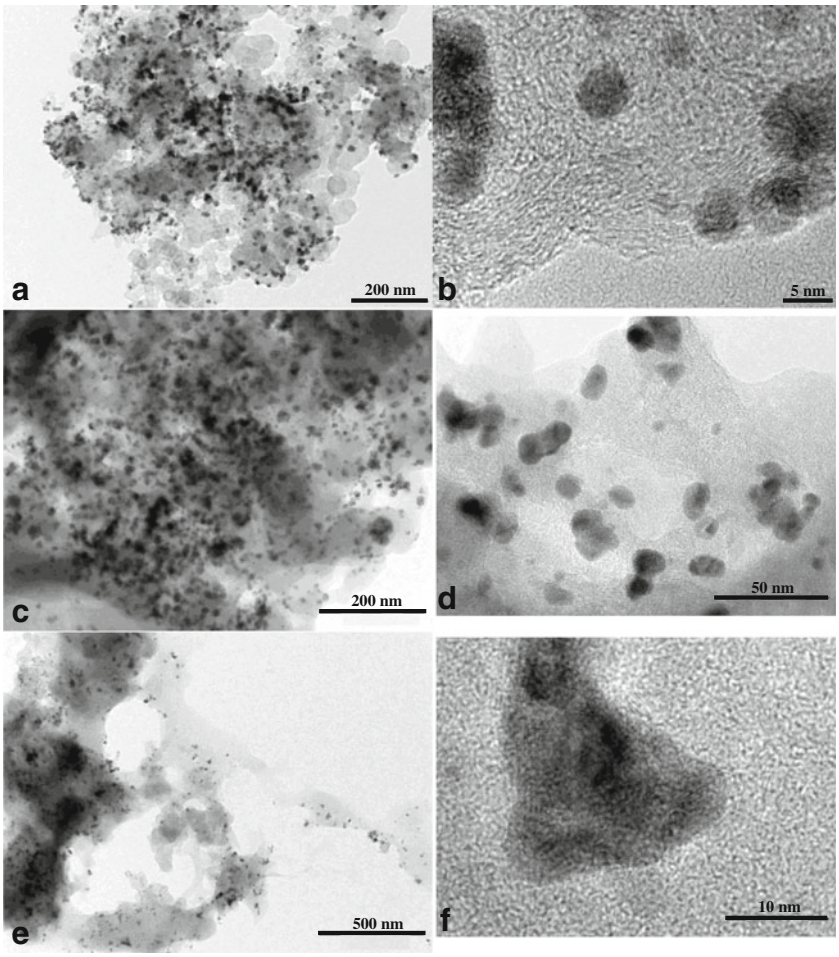

Fig. 2 Micrographs of TEM (*left*) and HRTEM (*right*) for Pd/C-0 (**a**, **b**), Pd/C-50 (**c**, **d**), and Pd/C-500 (**e**, **f**)

In this scenario, the electrochemical stability of NPs as a catalyst to fuel cells can be evaluated by monitoring the EASA [27]. The reduction of EASA under applied potentials is a diagnostic criterion of instability, as demonstrated by Strasser et al. in a series of recent papers [27–29].

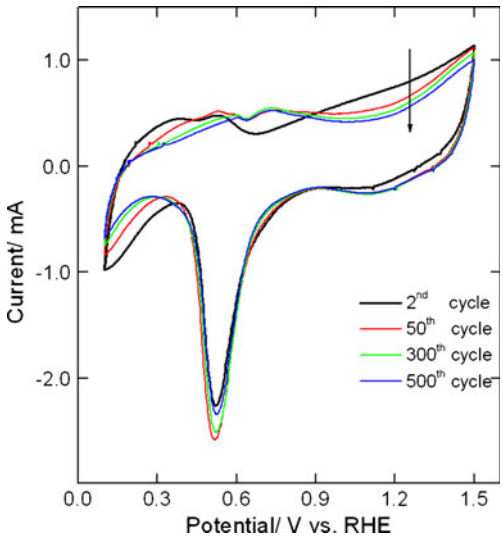

Fig. 3 Illustrative cyclic voltammograms recorded in the presence of NaOH 0.1 mol L^{-1} on Pd/C nanoparticle. v=0.1 V s^{-1}. The number of cycles is indicated in the figure

As an attempt to understand how the multiple processes (described in [15, 17, 30, 31]) taking place during the potential cycling might affect the assessment to the surface of the catalyst, we estimated the EASA by using the charge involved in the reduction of a PdO monolayer (from now on EASA-PdO) as 420 μC cm^{-2} [32]. The EASA-PdO was calculated after some representative cycles and normalized by the first area, EASA-PdO^0. Each normalized area corresponds to a dot in Fig. 4. Initially, the area of Pd/C (full symbols) abruptly increases up to the 80th cycle and then decays slightly until the 500th. The initial increase of area is probably associated to a cleaning process as observed in the voltammograms of Fig. 3. It is possible that some impurities (remanents from the synthesis) leave the surface during a particular cycle. Hence, those sites released become available to adsorb OH^- and to form PdO in the next cycle, leading to an increase of EASA-PdO. However, this process does not explain why the area decreases after the 80th cycle. The contribution of oxidation/dilution of Pd to the decrease of EASA-PdO cannot be ignored, but such diminution has a massive contribution of the agglomeration of particles which provokes an increase of their

average size (this phenomenon will be discussed later). Here is interesting to note that even using a different method of synthesis and a different catalyst, our results are qualitatively similar to those found by Strasser et al. [27]. These authors submit a Pt/C catalyst to 10,000 cycles up to 1.2 V and observed that the EASA increases until 200 cycles and then decays by a factor of 50 % after that [27]. In the present case, the EASA increasing is more pronounced than the corresponding lost (30 % vs. 14 %), but this is mainly explained by the lower number of cycles and due to the different NPs investigated in our study compared with that of Strasser et al. [27]. Figure 4 shows that there is no stabilization of the EASA-PdO values after the penultimate point, which indicates that probably EASA-PdO would keep decreasing if we performed more cycles.

In an attempt to eliminate eventual influence of the presence of PVP and glycolate, we manufactured a Pd electrodeposit on a gold disk. The conditions to obtain the Pd electrodeposit can be consulted elsewhere [33]. The electrodeposit was also submitted to 500 voltammetric cycles under the same conditions already described (Fig. 4, open stars). A small increase of the EASA-PdO is observed during the initial cycles, but it is far less evident than for the Pd/C. In general, the EASA-PdO decreases. Furthermore, the results of Pd electrodeposited agree with those previously observed by Tsuru et al. for Pt, who performed 300 cycles up to 1.4 V with electrodeposited Pt nanoparticles and observed a monotonous decay of the EASA [34]. Thereby, it seems clear that the impurities on Pd/C influence the behavior of the EASA-PdO.

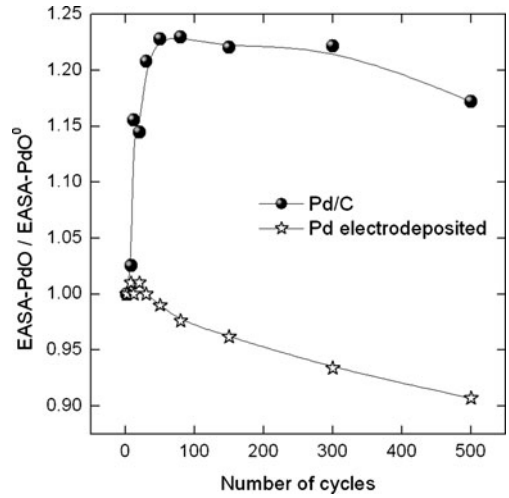

Fig. 4 Electrochemically active surface area (*EASA*) divided by the initial area for Pd/C (*spheres*) and Pd electrodeposited (*stars*) obtained by the charge of reduction of a PdO monolayer

The Effect of the Potential Cycling on CO Electrooxidation

We also investigated the electrooxidation of CO on Pd/C NPs by performing stripping of CO before the potential cycling and after 10, 20, 50, 100, 300, and 500 cycles (as shown the normalized curves in Fig. 5). The voltammogram after the CO electrooxidation reaction (COEOR) follows the trend shown in Fig. 3. On the fresh catalyst (black line), COEOR occurs in multiple steps. At ~0.47 V, a small shoulder can be discriminated (peak 1), followed by a more intense feature at 0.69 V (peak 2) and by a main oxidation peak at 0.82 V (peak 3). After 100 cycles, peak 3 diminishes while peak 2 becomes more pronounced and shifts to higher potentials (blue line in Fig. 5). After 500 cycles (magenta line), the potential of peak 3 slight decreases (~0.81 V), and the current for CO electrooxidation reaches their minimum values. At the same time, peak 2 becomes more and more accentuated, and peak 1 develops at ~0.53 V.

In this context, Feliu et al. investigated the effect of Pt NPs aggregation on CO electrooxidation and concluded that the proximity of the NPs increases the probability of the reaction among Pt(CO_{ad}) and Pt(OH_{ad}) species from different NPs [22]. According to these authors, such reaction occurs at relative low potentials and provokes the appearing of pre-peaks during CO electrooxidation [22]. Mayrhofer et al. investigated the influence of the particles size on the kinetics of COEOR [35]. These authors found that the onset potential of CO oxidation is barely dependent of the particle size; however, a huge increment of the NPs size (5 to 30 nm, at that study) displaces the onset potential toward significantly more negative values [35]. To explain our results, we also need to consider the adsorption of oxygenated groups on the edge-corner sites, which is stronger than on terraces over the surface [36, 37]. Therefore, the oxidation pre-peak can also be related to a reaction involving catalytically active OH formed on

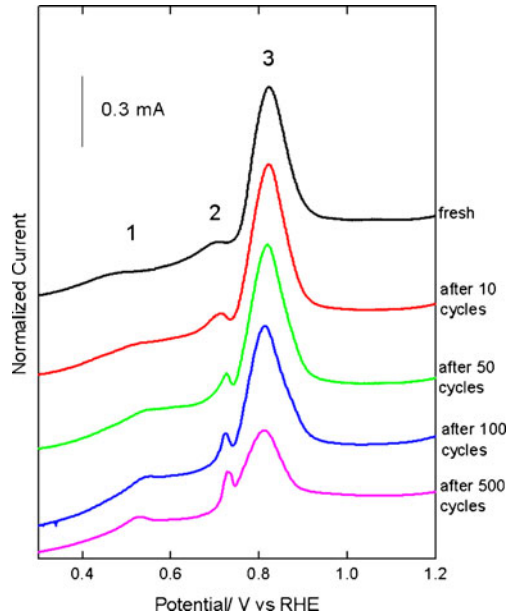

Fig. 5 Details of the anodic curves obtained during the CO electrooxidation on Pd/C NPs in NaOH 0.1 mol L^{-1} and at 0.02 V s^{-1}. The same catalyst was submitted to different cycles, indicated in the figure

defect sites and Pd-CO species on the surroundings of the edge, whereas the subsequent CO species diffuse toward the edge, which increase the overpotential for that reaction [38].

Apparently, agglomeration and morphology change effects can be used to explain our own results. Therefore, in the foregoing discussion, the results observed until now can be rationalized as a combination of an increasing availability of Pd sites (caused by a successive cleaning of the surface) and an agglomeration of the NPs with the potential cycling, which facilitates the reaction of CO with OH.

In order to confirm the agglomeration of Pd NPs, we performed TEM and HRTEM measurements to investigate three critical stages of the EASA-PdO curve seen in Fig. 4 (spheres): fresh catalyst (Pd/C-0), after 50 cycles (Pd/C-50), and after 500 cycles (Pd/C-500). Here we invoke Fig. 2 again to compare the average sizes and morphologies of Pd/C as a function of the potential cycling. The increase of the dark areas indicates some agglomeration of the NPs, as shown by Pd/C-50 and Pd/C-500 (Fig. 2c and e, respectively). Figure 2e was specially selected to show that despite the agglomeration, there are regions of the catalyst in which the NPs remain isolated. After the 50th cycle, an important collection of NPs seems to coalesce, and several pairs and groups of NPs join to create elliptical and shapeless NPs as those seen in Fig. 2d. After 500 cycles, the aggregation intensifies (Fig. 2f). Additional high-resolution micrographs of cycled NPs can be consulted in the supplementary information (Fig. S1). We can understand the agglomeration as a sum of two main effects: (a) migration and coalescence of Pd onto other NPs or onto a carbon defect and (b) diffusion of dissolved Pd followed by redeposition/reduction onto large NPs. These phenomena were previously investigated for Pt/C NPs [39] and confirmed by identical location transmission electron microscopy [17].

Aside from agglomeration, the successive cycles seems to provoke important changes in the morphology of the Pd NPs. Some small NPs might apparently reorganize by migration over the support and/or by Ostwald ripening to form larger polygonal NPs, as shown by the HRTEM image obtained after 500 cycles (Fig. 6). Some NPs also might suffer changes on the crystal lattice [40]. Both factors (agglomeration + reorganization) may contribute to changes in the electrochemical behavior in the absence and presence of CO, illustrated by Figs. 3 and 5, respectively. In function of the few number of NPs with the shape strongly modified (as shown in Fig. 6), we considered that the aggregation is the main responsible for the electrochemical behavior changes at the number of potential cycles studied.

This agglomeration, firstly reported here for Pd/C, increases the mean diameter of the NPs, as shown in the histograms of Fig. 7. A similar behavior was reported for Pt/C by Léger et al. [41]. The average diameters of Pd/C-0, Pd/C-50, and Pd/C-500 were 5.3±1.9, 9.2±2.8, and 11.6±3.6 nm,

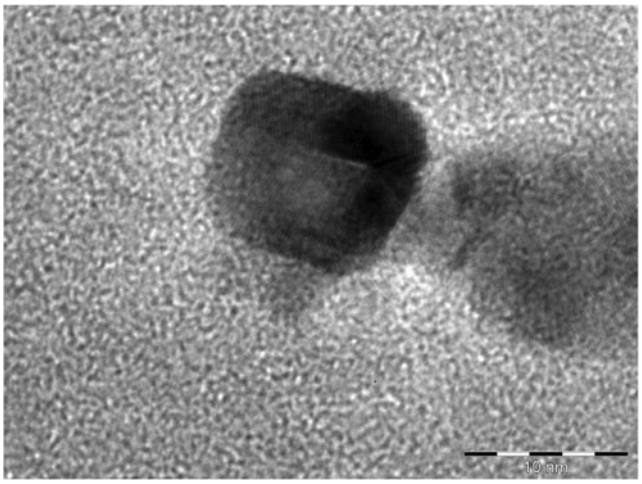

Fig. 6 Detail of a polygonal palladium nanoparticle. HRTEM image obtained after 500 voltammetric cycles

respectively. However, not all the particles experience agglomeration (as illustrated in Fig. 2e). Some NPs retain their original size, which led to an amplification of the distribution size, seen by the increase of the standard deviation and accordingly a broadening of the Gaussian curve (Fig. 7). The distribution ranges are 2–8.5 nm for Pd/C-0 and 5–23 nm for Pd/C-500. Therefore, the cycling procedure seems to promote the oxidation (or detachment) of PVP and impurities from Pd/C surface, then exposing nanoparticles, which, in turn, become suitable for agglomeration. The observed particle size increase is in line with the results of Fig. 5 and with the work of Mayrhofer et al. [35]. Namely, it does not seem enough for a negative onset potential shift of the main CO oxidation peak, but contributes to define the pre-peaks.

Based on our observations and results from literature for similar systems cited in this work, we can now suggest a relation between the complex behavior of CO stripping peaks and the Pd NPs surface structure:

1. Peak 3 seems to be mainly related to the electrooxidation of CO on isolated and small NPs. Such oxidation peak is a consequence of the reaction between CO_{ad} and OH_{ad} on the same NPs. This peak decreases as the nanoparticles agglomerate.
2. Conversely, peaks 1 and 2 show an opposite behavior: They grow as the NPs become cleaner, structurally modified, and agglomerated with the cycles. Therefore, these peaks seem to refer to reaction on larger NPs with a contribution of reactions among species on different NPs due to the agglomeration.

Additionally, we advertise the community about the implications of the use of the stripping of CO (EASA-CO) as a method to normalize the currents observed during electrochemical protocols, especially those ones obtained by

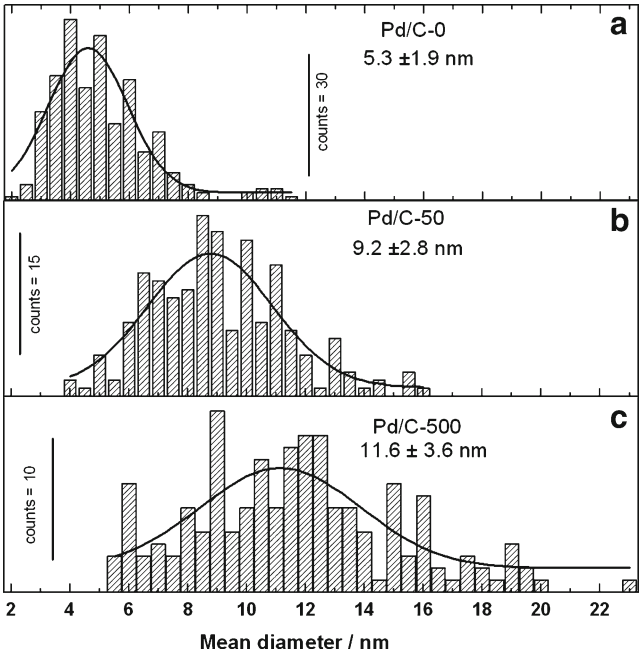

Fig. 7 Histograms obtained for *A* Pd/C-0, *B* Pd/C-50, and *C* Pd/C-500. Data extracted from TEM images like those ones shown in Fig. 2

synthetic routes that use surfactants and polymers (as in the present case). The next section is devoted to this issue.

Using Stripping of CO to Determine the Electrochemically Active Surface Area of NPs Synthetized by EG-PVP

The procedure of normalizing currents is mandatory in electrocatalysis, since it allows that different surfaces can be directly compared, providing a good guide to the determination of the intrinsic capability of a surface to catalyze a given reaction. Nevertheless, there is not a universal standardized method, and this choice is driven by the characteristics that the researchers intend to highlight. In fuel cell studies, it is usual to normalize the currents by the mass of the main catalyst [42]. For Pt-based catalysts, the EASA is usually estimated by the charge involved in the H desorption region [43, 44], while for Pd-based electrodes it is calculated from the charge involved in the reduction of the oxide monolayer [45]. However, it is consensual that the metal lattice parameter suffers drastic modifications when a foreign element is inserted inside its structure [46]. Hence, the charges involved in the electrochemical processes also change. In this context, it is consensual that the stripping of CO is a suitable method to normalize currents, mainly on surfaces that present a combination of metals [2]. In a recent study, van der Vliet et al. stated that the estimative of H_{upd} charge has to be compared to the charge of CO stripping in attempt to avoid neglecting the EASA of skin-type alloy catalysts [47].

Therefore, in the previous sections, we showed how the potential cycling might influence the electrooxidation of CO. Additionally, we follow the EASA-CO in function of the number of voltammetric cycles (open triangles in Fig. 8), and we observe a similar behavior to that one presented by EASA-PdO (Fig. 4). Then, we compare the EASA-CO with EASA-PdO obtained at the same cycle, as shown in Fig. 8. Initially, the values are of 9.1 and 7.2 cm^2 for EASA-PdO and EASA-CO, respectively. Moreover, EASA-CO increases up to the 50th cycle and then diminishes, whereas EASA-PdO (spheres in Fig. 8) decays continuously. Both methods furnish similar values for EASA between the 20th and the 50th cycles.

The behavior of EASA-PdO in Fig. 4 is quite distinct from the EASA-PdO in Fig. 8 (alternated CO stripping between cycles). Namely, EASA-PdO in Fig. 4 passes by a maximum while EASA-PdO in Fig. 8 decreases monotonously. According to Gong et al., the behavior of EASA-PdO in Fig. 8 can be understood in terms of a faster removal of PVP caused by the electrooxidation of CO [10]. Hence, CO_2 desorbs from the surface carrying important amounts of PVP and anticipates the cleaning process; on the other hand, in the absence of CO (Fig. 4), this cleanness requires more cycles to occur.

Now, if we assume that the cleaning of the surface is faster in the presence of CO, the remaining task is to explain why the values of EASA-CO and EASA-PdO are so different from the first to the 100th cycle. Concerning the electrooxidation of CO, it seems plausible that during the continuous process of agglomeration there is a balance between the gain of active sites able to promote the oxidation of CO over different NPs and the loss of area provoked by the growing of the particles. Hence, the apparent area seems to increase because more CO is oxidized, even that the surface able to the reaction is becoming smaller. Eventually, the decreasing of area prevails and we see an inflection point for the EASA-CO in Fig. 8 (around the 100th cycle). From this point onward, both the values of EASA become increasingly similar. On the other

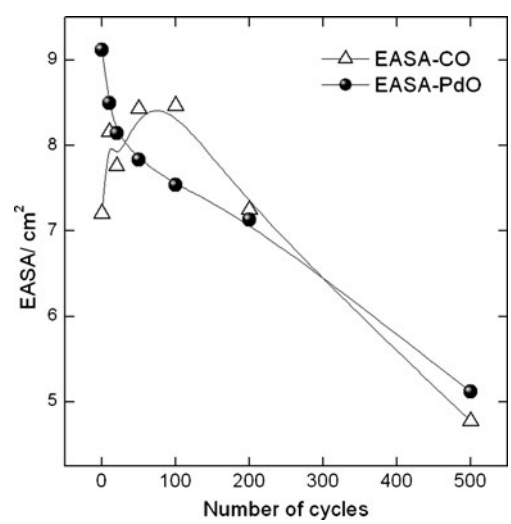

Fig. 8 Comparison of the electrochemically active surface area of Pd/C nanoparticles calculated from the charge involved in the stripping of CO (*open triangles*) and the reduction of the PdO (*spheres*)

hand, the reduction of PdO is not fostered by the agglomeration of nanoparticles because in that case there is no need of a reaction partner in the neighborhood (i.e., on surrounding particles). Consequently, the only apparent effect is the decrease of the area available for the reduction of PdO.

Finally, it is important to highlight that the choice of a particular method to normalize the electroactive area of a catalyst must obey to a judicious protocol, which means that when a method is used, the normalized current must refer to the same surface condition. In this context, our results demonstrate that the presence of impurities on the surface of nanoparticles could be an explanation for contradictory results usually found in the literature for similar systems.

Conclusions

- Pd/C nanoparticles obtained by EG-PVP method contain impurities on surface, which can be removed by cycling the potential. However, this cleaning is accompanied by agglomeration and structural modifications of the nanoparticles, which changes the electrochemical behavior of the catalyst.
- When a Pd electrodeposit is submitted to the same conditions adopted for Pt/C, only a small increase of area is perceived during the first cycles, followed by a decrease of EASA. These observations reinforce our hypothesis that the impurities present on Pd/C influence the behavior of the EASA-PdO.
- The general features of the multiple CO electrooxidation peaks continuously change after successive voltammetric cycles. Results are rationalized in terms of the occurrence of interparticle reactions when the particles agglomerate, which favors the reaction of CO and OH from different NPs in addition to reaction on the same NPs, however involving a possibly crystalline and defect modified surface.
- The size and morphology changes of Pd/C NPs during the potential cycling modified the CO electrooxidation reaction. This evidence probably might be extended to more complex reaction, as methanol and ethanol electrooxidation taking place on Pd-alloy catalysts.
- The initial active surface areas for Pd/C fresh catalysts are quite different from those obtained after several voltammetric cycles, regardless they were obtained by stripping of CO or by the charge involved in the reduction of PdO. Such discrepancies indicate a continuous change of the electrochemically active surface area as the voltammetric cycles are performed. Consequently, the use of the active area for purposes of normalization of the currents must be conducted in a particular superficial condition.
- Data concerning the determination of the electrochemically active surface area obtained for Pd/C show different values when the charges involved in CO oxidation and PdO reduction are compared, especially when the particles are still recovered (i.e., at the beginning of the cycling protocol). Such differences are rationalized in terms of a balance between the increase of sites which promote the CO oxidation and the loss of area provoked by the growing of the particles.

Acknowledgments The authors acknowledge financial assistance from Consejo Nacional de Investigaciones Científicas y Técnicas (CONICET), UNLP, CNPq (grant # 554591/2010-3), FUNDECT (grants # 23/200.065/2008 and # 23/200.583/2012), CAPES, MINCyT, and FINEP. P.S. Fernández thanks CONICET for a fellowship. C.A. Martins thanks CNPq for a fellowship (grant # 140426/2011-6). Authors want to thank Alejandra Floridia for taking HR-TEM images.

References

1. M. Watanabe, S. Motoo, J. Electroanal. Chem. **60**, 275 (1975)
2. Y.C. Wei, C.W. Liu, W.D. Kang, C.M. Lai, L.D. Tsai, K.W. Wang, J. Electroanal. Chem. **660**, 64 (2011)
3. Y. Bi, L. Chen, G. Lu, J. Mol. Catal. A Chem. **266**, 173 (2007)
4. M. Chen, Y. Xing, Langmuir **21**, 9334 (2005)
5. P.S. Fernández, M.E. Martins, G.A. Camara, Electrochim. Acta **66**, 180 (2012)
6. H. Hei, H. He, R. Wang, X. Liu, G. Zhang, Soft Nanosci. Lett. **2**, 34 (2012)
7. C. Susut, T.D. Nguyen, G.B. Chapman, Y. Tong, Electrochim. Acta **53**, 6135 (2008)
8. D. Li, C. Wang, D. Tripkovic, S. Sun, N.M. Markovic, V.R. Stamenkovic, ACS Catal. **2**, 1358 (2012)
9. A. Goel, N. Rani, Open J. Inorg. Chem. **2**, 67 (2012)
10. K. Gong, M.B. Vukmirovic, C. Ma, Y. Zhu, R.R. Adzic, J. Electroanal. Chem. **662**, 213 (2011)
11. L.H.S. Gasparotto, J.F. Gomes, G. Tremiliosi-Filho, J. Electroanal. Chem. **663**, 48 (2011)
12. A.M. Hofstead-Duffy, D.J. Chen, Y.J. Tong, Electrochim. Acta **82**, 543 (2012)
13. C. Coutanceau, P. Urchaga, S. Brimaud, S. Baranton, Electrocatal. **3**, 75 (2012)
14. J. Solla-Gullon, V. Montiel, A. Aldaz, J. Clavilier, J. Electroanal. Chem. **491**, 69 (2000)
15. P.S. Fernández, D.S. Ferreira, C.A. Martins, H.E. Troiani, G.A. Camara, M.E. Martins, Electrochim. Acta **98**, 25 (2013)
16. P.L. Redmond, A.J. Hallock, L.E. Brus, Nano Lett. **5**, 131 (2005)
17. F.R. Nikkuni, E.A. Ticianelli, L. Dubau, M. Chatenet, Electrocatal. **4**, 104 (2013)
18. O.V. Chertiouk, P.A. Simonov, E.R. Savinova, Electrochim. Acta **48**, 3851 (2003)
19. F. Maillard, E.R. Savinova, P.A. Simonov, V.I. Zaikovskii, U. Stimming, J. Phys. Chem. B **108**, 17893 (2004)
20. F. Maillard, E.R. Savinova, U. Stimming, J. Electroanal. Chem. **599**, 221 (2007)
21. G.A. Camara, J.F. Gomes, K. Bergamaski, E. Teixeira-Neto, F.C. Nart, J. Electroanal. Chem. **617**, 171 (2008)
22. A. López-Cudero, J. Solla-Gullón, E. Herrero, A. Aldaz, J.M. Feliu, J. Electroanal. Chem. **644**, 117 (2010)
23. S. Park, S.A. Waisileski, M.J. Weaver, J. Phys. Chem. B **105**, 9719 (2001)

24. S. Park, Y.J. Tong, A. Wieckowski, M.J. Weaver, Langmuir **18**, 3233 (2002)
25. R. Lamber, S. Wetjen, N.I. Jaeger, Phys. Rev. B Solid State **51**, 10968 (1995)
26. A.E. Bolzán, J. Electroanal. Chem. **380**, 127 (1995)
27. A. Marcu, G. Toth, R. Srivastava, P. Strasser, J. Power Sources **208**, 288 (2012)
28. F. Hasché, M. Oezaslan, P. Strasser, ChemCatChem **3**, 1805 (2011)
29. F. Hasche, M. Oezaslan, P. Strasser, Phys. Chem. Chem. Phys. **12**, 15251 (2010)
30. W.J. Plieth, J. Phys. Chem. **86**, 3166 (1982)
31. L. Tang, B. Han, K. Persson, C. Friesen, T. He, K. Sieradzki, G. Ceder, J. Am. Chem. Soc. **132**, 596 (2009)
32. H.A. Kozlowska, J.O.'.M. Bockris, in *Comprehensive Treatise of Electrochemistry*, ed. by E.B. Yeager, B.E. Conway, S. Sarangapani, vol. 9 (Plenum, New York, 1984), p. 2
33. R.S. Ferreira Jr., M.J. Giz, G.A. Camara, J. Electroanal. Chem. **697**, 15 (2013)
34. Y. Sugawara, A.P. Yadav, A. Nishikata, T. Tsuru, J. Electroanal. Chem. **662**, 379 (2011)
35. K.J.J. Mayrhofer, M. Arenz, B.B. Blizanac, V. Stamenkovic, P.N. Ross, N.M. Markovic, Electrochim. Acta **50**, 5144 (2005)
36. J.S. Spendelow, J.D. Goodpaster, P.J.A. Kenis, A. Wieckowski, J. Phys. Chem. B **110**, 9545 (2006)
37. B. Hammer, O.H. Nielsen, J.K. Norskov, Catal. Lett. **46**, 31 (1997)
38. M. Arenz, K.J.J. Mayrhofer, V. Stamenkovic, B.B. Blizanac, T. Tomoyuki, P.N. Ross, N.M. Markovic, J. Am. Chem. Soc. **127**, 6819 (2005)
39. Y.S. Horn, W.C. Sheng, S. Chen, P.J. Ferreira, E.F. Holby, D. Morgan, Top. Catal. **46**, 285 (2007)
40. J. Clavilier, D. Armand, J. Electroanal. Chem. **199**, 187 (1986)
41. C. Grolleau, C. Coutanceau, F. Pierre, J.-M. Léger, Electrochim. Acta **53**, 7157 (2008)
42. Z. Cui, P.J. Kulesza, C.M. Li, W. Xing, S.P. Jiang, Int. J. Hydrogen Energy **36**, 8508 (2011)
43. C. Hsu, C. Huang, Y. Hao, F. Liu, Phys. Chem. Chem. Phys. **14**, 14696 (2012)
44. R. Lin, C. Cao, H. Zhang, H. Huang, J. Ma, Int. J. Hydrogen Energy **37**, 4648 (2012)
45. C. Hsu, C. Huang, Y. Hao, F. Liu, Electrochem. Commun. **23**, 133 (2012)
46. E. Antolini, J. Power Sources **170**, 1 (2007)
47. D.F. van der Vliet, C. Wang, D. Li, A.P. Paulikas, J. Greeley, R.B. Rankin, D. Strmcnik, D. Tripkovic, N.M. Markovic, V.R. Stamenkovic, Angew. Chem. **124**, 3193 (2012)